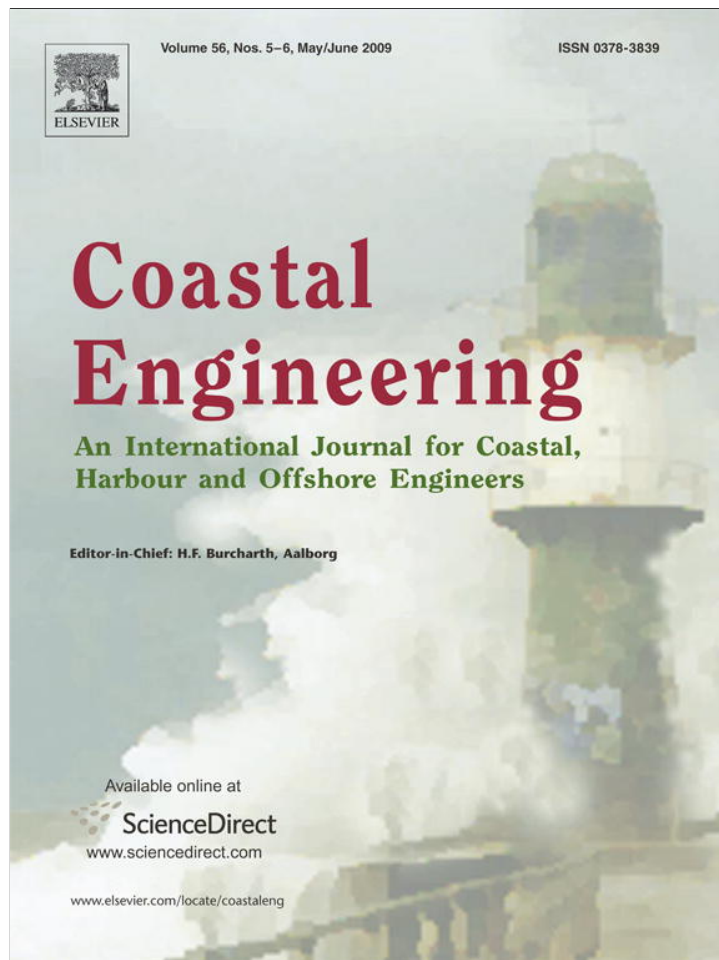


Provided for non-commercial research and education use.
Not for reproduction, distribution or commercial use.



This article appeared in a journal published by Elsevier. The attached copy is furnished to the author for internal non-commercial research and education use, including for instruction at the authors institution and sharing with colleagues.

Other uses, including reproduction and distribution, or selling or licensing copies, or posting to personal, institutional or third party websites are prohibited.

In most cases authors are permitted to post their version of the article (e.g. in Word or Tex form) to their personal website or institutional repository. Authors requiring further information regarding Elsevier's archiving and manuscript policies are encouraged to visit:

<http://www.elsevier.com/copyright>



Contents lists available at ScienceDirect

Coastal Engineering

journal homepage: www.elsevier.com/locate/coastaleng

The form of the asymptotic depth-limited wind-wave spectrum Part II – The wavenumber spectrum

I.R. Young*, A.V. Babanin

Engineering and Industrial Sciences, Swinburne University of Technology, Melbourne, Australia

ARTICLE INFO

Article history:

Received 26 July 2008

Received in revised form 15 November 2008

Accepted 18 November 2008

Available online 20 December 2008

Keywords:

Wavenumber spectrum

Finite depth waves

Non-linear waves

Lake George

Wavelet Directional Method

ABSTRACT

Data from a spatial array of wave gauges is analysed using the Wavelet Directional Method (WDM) to directly determine the wavenumber spectrum. The data shows that the asymptotic depth-limited wavenumber spectrum can be represented as a two-parameter form, which is far simpler than the corresponding frequency spectrum. The WDM analysis shows that there are significant nonlinear processes active in the finite depth water, which results in energy being “smeared” across a range of wavenumbers and frequencies around the standard dispersion shell. As a result, the wavenumber spectrum has much less peak enhancement than seen in the frequency spectrum obtained with standard Fourier analysis. In addition, the wavenumber spectrum does not have the clear harmonic previously observed in the finite depth frequency spectrum. This result demonstrates that the harmonic is nonlinearly phase-locked to the spectral peak.

© 2008 Elsevier B.V. All rights reserved.

1. Introduction

The asymptotic depth-limited spectral form is the limiting surface wave spectrum which would be generated by wind of a given strength blowing over a large area of uniform finite depth water. As such, this spectral form represents an important limiting condition for engineering design. The form of the spectrum also provides an important insight into the physical processes responsible for wind-wave generation and decay, as the limiting form represents a balance between the known processes of atmospheric input, nonlinear four-wave interactions, white-cap dissipation, bottom friction and three-wave finite depth nonlinear processes.

There are numerous measurements of wave spectra in finite depth conditions (e.g. Thompson, 1980; Bouws et al., 1985, 1987; Vincent, 1985; Resio, 1988; Miller and Vincent, 1990). All of these observations are, however, of oceanic waves which have propagated into finite depth water, having been previously generated in deep-water. As such, the spectral balance is different from the present situation. Waves propagating from deep to shallow water evolve due to the effects of shoaling and the dissipative mechanisms of wave breaking and bottom friction. In contrast, wave generation in relatively constant water depth represents a balance of the processes of atmospheric input, nonlinear interactions and dissipation due to bottom friction and wave breaking. Observations of waves generated in such finite depth conditions are much rarer (Thijssse, 1949; U.S. Army Corps of Engineers, 1955; Bretschneider, 1958; Young and Verhagen, 1996a). These observations concentrate on the integral spectral properties of

total energy and peak frequency, rather than the form of the spectrum. Observations of the full spectrum are largely confined to the measurements in Lake George (Young and Verhagen, 1996b; Young et al., 1996; Resio et al., 2004; Young and Babanin, 2006) and the recent observations in Lake IJssel (Bottema, 2007).

These shallow-water observations have been in the form of time series from which the frequency spectrum can be directly obtained, although it has been recognized that in finite depth conditions the wavenumber spectrum is probably a more appropriate representation (Bouws et al., 1987; Miller and Vincent, 1990; Young and Babanin, 2006). Attempts to define the wavenumber form in finite depth conditions have relied on transforming the frequency spectrum with an assumed (linear) dispersion relation, rather than measuring the wavenumber form directly. As waves in finite depth conditions are likely to be nonlinear, the assumption that the frequency spectrum can be transformed in this manner is questionable. Hence, the validity of such inferred wavenumber spectra needs to be investigated.

The most detailed of these previous observations are those of Young and Babanin (2006) (henceforth called Part I). These measurements were made using a spatial array of capacitance gauges, although the Young and Babanin (2006) analysis used only a single gauge to form the frequency spectrum. The current paper will extend the analysis of Part I by directly determining the wavenumber spectrum from the spatial array using the Wavelet Directional Method (WDM) described by Donelan et al. (1996). This analysis, combined with that of Part I provides a full description of the asymptotic depth-limited spectrum in both frequency and wavenumber space and provides insight into the nonlinear processes active in these conditions.

The arrangement of the paper is as follows. Section 2 provides a brief description of previous observations, with particular reference to the

* Corresponding author. Swinburne University of Technology, P.O. Box 218, Hawthorn, Vic 3122, Australia.

E-mail address: iyoung@swin.edu.au (I.R. Young).

wavenumber spectrum. Section 3 describes the experimental configuration and data collected. An important element of this paper is the WDM analysis and this technique and the data analysis are described in Section 4. Section 5 provides a comprehensive analysis of the data and a parametric representation of the wavenumber spectrum. Discussion of the results and conclusions are made in Section 6.

2. Observations of the depth-limited spectrum

Part I provides a detailed description of previous observations of both the integral parameters of the spectrum and the spectrum itself in finite depth conditions. An abbreviated form is repeated here with particular concentration on the wavenumber spectrum. Such wind-generated finite depth observations typically consider the integral properties of total energy, $E = \int F(f)df$ and peak spectral frequency, f_p , where $F(f)$ is the frequency spectrum and $f = \omega/2\pi$ is the frequency and ω the angular frequency. In wavenumber space, the corresponding quantities become, $E = \int F(k)dk$ and the peak spectral wavenumber, k_p , where $F(k)$ is the omnidirectional wavenumber spectrum [note that $E = \int F(f)df = \int F(k)dk$ and $k = |k|$ is the modulus of the wavenumber vector. These parameters are typically represented in non-dimensional form as: nondimensional energy $\varepsilon = g^2 E / U_{10}^4$, nondimensional peak frequency $\nu = f_p U_{10} / g$ and nondimensional wavenumber $\kappa = U_{10}^2 k_p / g$, where U_{10} is the wind speed measured at a reference height of 10 m. As discussed in Part I, the friction velocity, u_* and the wind speed at a reference height of one-half a wavelength $U_{\lambda/2}$ have also been proposed as scaling wind speeds (Young, 1999). In the present analysis, U_{10} has been chosen for the pragmatic reason that it is the quantity which is most often available in the field.

Young and Babanin (2006) determined asymptotic limits to these quantities of the form

$$\varepsilon_d = 1.0 \times 10^{-3} \delta^{1.2} \quad (1)$$

and

$$\kappa_d = 1.80 \delta^{-0.73} \quad (2)$$

where $\delta = gd / U_{10}^2$ is the nondimensional depth and the subscript d signifies that this is the asymptotic depth-limited value. Hence, ε_d , κ_d and ν_d are the depth-limited values of nondimensional energy, wavenumber and frequency, respectively.

Importantly, Young and Babanin (2006) could not find a similar relationship between ν_d and δ which was applicable over the full parameter range of their data. This result led Young and Babanin (2006) to postulate that the wavenumber spectrum may be the most appropriate spectral form to describe the data. As their analysis could not directly determine $F(k)$, they could not investigate this possibility.

Young and Babanin (2006) considered spectra for which both ε and κ were within $\pm 20\%$ of the limits defined by Eqs. (1) and (2) respectively and considered these spectra to be at the finite depth asymptotic limit. These frequency spectra appeared similar to typical deep water spectra but had a consistent small harmonic at approximately $2f_p$ which was interpreted as the result of 3-wave or triad nonlinear interactions. Young and Babanin (2006) parameterized this “two-peak” form by

$$F(f) = F_1(f) + F_2(f) \quad (3)$$

where

$$F_1(f) = \beta_1 g^2 (2\pi)^{-4} f_p^{-(5+n_1)} f^{n_1} \exp\left[\frac{n_1}{4} \left(\frac{f}{f_{p1}}\right)^{-4}\right] \cdot \gamma_1 \exp\left[\frac{-(f-f_{p1})^2}{2\sigma_1^2 \beta_1}\right] \quad (4)$$

$$F_2(f) = \beta_2 g^2 (2\pi)^{-4} f_p^{-(5+n_2)} f^{n_2} \exp\left[\frac{n_2}{4} \left(\frac{f}{f_{p2}}\right)^{-4}\right] \quad (5)$$

The parameters in Eqs. (4) and (5) were defined by

$$\beta_1 = 5.89 \times 10^{-3} \delta^{0.085} \quad (6)$$

$$\gamma_1 = 2.97 \times 10^{-3} \beta_1^{-1.34} \quad (7)$$

$$\sigma_1 = 2.0 \times 10^{-6} \beta_1^{-2.09} \quad (8)$$

and $n_1 = -4$, $n_2 \approx -8.35$ and $\beta_2 \approx 0.074$.

The system of Eqs. (3)–(8) fully defines the spectrum given the water depth, d and wind speed U_{10} . Although these relationships model the observed frequency spectra well, the complex two-peak spectral form is a purely empirical approximation to the data. The frequency spectral (Fourier) form is usually interpreted as a summation of independent spectral components, each propagating at its local phase velocity. This is not the case for finite depth waves, where the harmonic is not a free wave, but is phase-locked to the spectral peak and propagates at the phase speed of the peak. In reality there are not two sinusoidal waves with frequencies f_p and $2f_p$, but a single non-sinusoidal (Stokes-like) wave of frequency f_p (or wavenumber k_p). This feature, together with the wavenumber scaling of the asymptotic relationship Eq. (2) and the absence of Doppler smearing suggests that the wavenumber spectrum, $F(k)$, may be a more appropriate representation for the asymptotic form.

The wavenumber spectrum has previously been proposed for the modelling of finite depth spectra. Based on the assumption that the high wavenumber region of the spectrum is the result of a constant flux of energy through the spectrum from 4-wave nonlinear interactions, Kitaigorodskii et al. (1975) were able to show that the wavenumber spectrum takes the form

$$F(k) \propto k^{-3} \quad (9)$$

Eq. (9) holds irrespective of the water depth, provided that the assumption that the high wavenumber region is the result of 4-wave nonlinear interactions, remains valid. Bouws et al. (1985) extended Eq. (9) to develop a full finite depth spectral representation, termed the TMA spectrum.

Eq. (9) yields a frequency spectrum proportional to f^{-5} in deep water and f^{-3} at the shallow water limit. Based on the fact that many deep water observations yield a form proportional to f^{-4} , Miller and Vincent (1990) questioned the validity of Eq. (9) and instead proposed

$$F(k) \propto k^{-2.5} \quad (10)$$

Similar forms were also proposed by Kitaigorodskii (1983) and Phillips (1985). Miller and Vincent (1990) termed Eq. (10) the FRF spectrum, which asymptotes to a deep water frequency form proportional to f^{-4} , consistent with the observational data.

Theoretical support for the $k^{-2.5}$ form in finite depth water has been provided by Resio et al. (2001), who showed that this form results from a constant flux of energy to higher frequencies, analogous to the Kolmogorov cascade which occurs in turbulence. Experimental evidence from the surf zone (Smith and Vincent, 1992, 2002) suggests that two ranges may exist, with $k^{-4/3}$ (consistent with the theory of Zakharov (1999) for shallow water), for lower values of k_d , and a transition to $k^{-2.5}$ for $k_d > 1$.

As noted by Vincent (1984), the TMA (or FRF) form is attractive, as the water depth is included explicitly through the wavenumber. The strict validity of the form may however, be limited by the assumption of the high wavenumber tail being maintained by a constant flux of energy through the spectrum. As water depth varies, the source term balance also changes with all terms (input, dissipation, 4-wave nonlinear and bottom friction) increasing in magnitude. In addition, 3-wave interactions also become important, as evidenced by the harmonic in Eq. (3). Therefore, although the general argument for

representation of the finite depth spectral form in wavenumber space still holds, the exact forms proposed by Bouws et al. (1985), Miller and Vincent (1990) or Resio et al. (2001) may not strictly hold.

3. Experimental configuration and recorded data

Wave data were collected in Lake George in south-eastern Australia. This site has been well documented in the previous studies of Young and Verhagen (1996a,b) and Young et al. (1996). The measurements were made from a platform on the eastern shore of the lake. This experimental site and the instrumentation and data recorded for this experiment have been reported in detail in Young et al. (2005) and in Part I. A broad range of environmental parameters were recorded as part of the full experimental program. Of particular relevance to this study, coincident measurements of the water surface elevation, water depth and wind speed at a reference height of 10 m were made. The water surface elevation measurements were made using a spatial array in the form of a centred pentagon of radius 15 cm. Fig. 1a shows the configuration of gauges and Fig. 1b shows a photograph of the array. The probes in the array were coincidentally sampled at 25 Hz, records consisting of 20 min duration (i.e. 30,000 samples per probe). This array data was analysed using the WDM method (see Section 4) to obtain wavenumber spectra. All other details of the experimental configuration can be found in Part I.

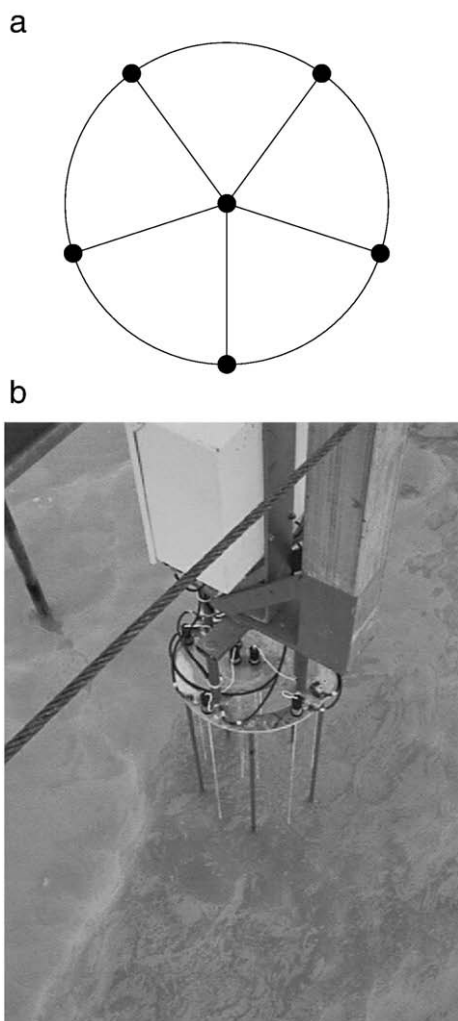


Fig. 1. (a) The spatial array of capacitance wave gauges. The array is in the form of a centred pentagon of radius, 15 cm. (b) A photograph of the array of (a) deployed during the experiment.

As described in Section 4, it is desirable for the array to have a small foot print, as this reduces errors caused by multiple wavelets being within the array footprint at the same time and also improves the high wavenumber limit. However, as the array size decreases, the accuracy with which low wavenumbers can be resolved reduces. The array wires have a diameter of 1 mm. Hence, with a diameter of 300 mm for the array, the slope accuracy is $\pm 0.5/300 = 0.0017$. Typical spectra recorded during the experiment had a peak wavenumber, $k_p = 0.8$ rad/m or wavelength of 7.8 m and a peak frequency, $f_p = 0.4$ Hz. Noting that the sampling rate of the array was 25 Hz, the accuracy with which the wave height could be determined becomes $\Delta H = \pm 7.8 \times 0.0017 / (2.5 \times 25) = \pm 0.212$ mm. Hence, with a typical wave height of 0.3 m, the potential error is $\pm 0.07\%$ at the spectral peak. Although this error increases with decreasing wavenumber, the error remains small over the full range of data considered.

The high wavenumber limit of the array is also limited by array size. With an array of 300 mm, the highest wavenumber which can be resolved without aliasing is $k = 2\pi/0.3 = 21$ rad/m. This corresponds to a high frequency limit of $f = 2.3$ Hz. In the present analysis, spectra were only considered up to $k = 10$ rad/m, thus ensuring that the upper wavenumber limit was not exceeded.

The wave probe records were sub-divided into blocks of 256 points and the wavelets formed using an analysis with 8 voices. The wavelet analysis considers the wave field to be made up of a summation of independent Morlet wavelets, each of different scale (Donelan et al., 1996). To improve accuracy, it is common to carry out the analysis at additional intermediate scales, called voices. The number of voices was varied between 4 and 12 with little impact on the resulting spectra. Part I presented a detailed analysis of the confidence limits associated with the resulting spectra. Such an analysis is beyond the scope of this paper, as the statistical variability of WDM derived spectra is yet to be determined. However, 6 times as much data is used to derive each spectrum in the WDM analysis compared to the Fourier analysis of Part I. Therefore, it is reasonable to assume that the confidence limits will not be larger than those for Part I (i.e. the upper and lower 95% confidence limits are given by $1.3 F(k)$ and $0.8 F(k)$, respectively, where $F(k)$ is the estimate of the spectral ordinate).

The data employed in this paper were recorded over an approximately 1 year period between September 1997 and October 1998 (full details of all recorded time series are given in Part I). A total of 55 records were used in the WDM analysis, the parameters associated with each of the records is summarised in Table 1. This is less than the 92 records used in Part I since it was necessary for all 6 probes in the array to be operating correctly in order to apply the WDM analysis. As detailed in Part I and above, records which are considered to be at the asymptotic depth-limited condition are identified in Table 1 with a Depth Flag value of 1.

4. The Wavelet Directional Method

The direct measurement of the directional wavenumber spectrum, $F(\underline{k})$, where \underline{k} is the wavenumber vector is a challenging undertaking. The most obvious approach is to define the two dimensional surface elevation over a spatial domain. Because of the need to resolve long wavelengths, this is a particularly challenging instrumentation problem. The most common approach has been through stereo-photography (e.g. Holthuijsen, 1983; Banner et al., 1989). Such approaches have difficulty imaging a large enough region, whilst maintaining sufficiently high resolution to be able to resolve the full wavenumber range of the spectrum. Remote sensing techniques have also been applied to the problem (e.g. Alpers et al., 1981; Young et al., 1985; Hasselmann et al., 1985). Such systems have great potential but rely upon still incomplete knowledge of complex transfer functions and other factors relating the image spectrum to the wave spectrum.

Table 1
Summary data used in WDM analysis^a.

	Date ^b	δ	ε	κ	H_s (m)	f_p (Hz)	U_{10} (m/s)	d (m)	$k_p d$	U_r	F_c	Depth flag
1	c010204.no7	4.86e-002	2.13e-005	17.11	0.338	0.398	13.400	0.89	0.832	21.7	124	1
2	c010226.no7	4.57e-002	2.25e-005	17.93	0.374	0.391	13.900	0.90	0.819	24.4	134	1
3	c010248.no7	4.17e-002	1.93e-005	19.97	0.392	0.389	14.800	0.93	0.832	24.0	131	1
4	c011210.oc8	1.15e-001	4.97e-005	9.90	0.233	0.493	9.000	0.95	1.14	7.45	53.8	0
5	c011245.oc8	9.51e-002	4.28e-005	10.45	0.261	0.444	9.900	0.95	0.994	11.0	73.9	0
6	c011323.oc8	8.96e-002	5.09e-005	10.21	0.303	0.416	10.200	0.95	0.915	15.0	93.6	1
7	c011406.oc8	7.56e-002	3.49e-005	12.18	0.297	0.418	11.100	0.95	0.921	14.5	91.5	1
8	c011445.oc8	5.43e-002	2.13e-005	15.70	0.323	0.393	13.100	0.95	0.852	18.5	112	0
9	c031151.se8	2.78e-001	1.62e-004	5.42	0.169	0.607	5.700	0.92	1.50	3.20	28.7	1
10	c031214.se8	2.35e-001	1.19e-004	5.89	0.171	0.574	6.200	0.92	1.38	3.84	33.3	0
11	c031243.se8	2.56e-001	1.25e-004	5.55	0.159	0.589	5.900	0.91	1.42	3.41	30.7	0
12	c031307.se8	2.01e-001	1.15e-004	6.78	0.196	0.569	6.700	0.92	1.36	4.53	36.5	1
13	c031331.se8	1.16e-001	5.27e-005	9.98	0.234	0.502	8.900	0.94	1.16	7.29	52.3	0
14	c031356.se8	1.64e-001	1.13e-004	7.06	0.243	0.501	7.500	0.94	1.16	7.64	53.8	1
15	c031419.se8	2.51e-001	1.76e-004	4.76	0.195	0.518	6.000	0.92	1.19	5.88	46	1
16	c031442.se8	2.75e-001	1.96e-004	4.54	0.185	0.537	5.700	0.91	1.25	5.16	41.6	1
17	c061151.oc8	5.46e-002	2.21e-005	16.56	0.334	0.408	13.200	0.97	0.905	16.6	99.6	0
18	c061234.oc8	6.09e-002	2.14e-005	15.29	0.294	0.417	12.500	0.97	0.931	13.8	88.2	0
19	c061323.oc8	5.38e-002	2.18e-005	16.71	0.336	0.406	13.300	0.97	0.899	16.9	101	0
20	c061425.oc8	5.07e-002	1.99e-005	16.74	0.341	0.387	13.700	0.97	0.849	19.3	114	0
21	c111051.oc7	6.72e-002	1.66e-005	28.16	0.276	0.628	12.900	1.14	1.89	2.67	23.2	0
22	c111124.oc7	6.83e-002	1.77e-005	27.78	0.281	0.629	12.800	1.14	1.90	2.71	23.3	0
23	c111156.oc7	7.04e-002	1.87e-005	24.56	0.280	0.596	12.600	1.14	1.73	3.24	26.7	0
24	c111224.oc7	7.90e-002	2.02e-005	23.46	0.259	0.620	11.900	1.14	1.85	2.62	23.2	0
25	c111402.oc7	6.62e-002	1.62e-005	27.30	0.277	0.611	13.000	1.14	1.81	2.94	24.9	0
26	c111538.oc7	8.31e-002	2.09e-005	23.95	0.251	0.647	11.600	1.14	1.99	2.19	20.6	0
27	c141237.no7	6.68e-002	2.72e-005	13.10	0.306	0.395	12.000	0.98	0.875	16.1	102	0
28	c141259.se8	9.14e-002	3.11e-005	13.32	0.232	0.517	10.100	0.95	1.22	6.51	47.6	0
29	c141305.no7	4.93e-002	1.82e-005	18.06	0.346	0.397	14.100	1.00	0.891	17.2	103	0
30	c141328.no7	4.89e-002	1.82e-005	17.60	0.356	0.382	14.300	1.02	0.861	18.6	111	0
31	c141351.no7	4.85e-002	1.95e-005	18.13	0.379	0.385	14.500	1.04	0.88	18.6	108	1
32	c141358.se8	8.29e-002	2.89e-005	13.73	0.246	0.492	10.600	0.95	1.14	7.88	55.4	0
33	c141415.no7	4.29e-002	1.37e-005	19.86	0.362	0.373	15.500	1.05	0.851	18.8	113	0
34	c141448.se8	1.08e-001	3.39e-005	13.23	0.205	0.577	9.300	0.95	1.43	4.2	34.1	0
35	c141502.se8	9.90e-002	3.44e-005	11.62	0.225	0.496	9.700	0.95	1.15	7.06	51.9	0
36	c151238.de7	6.53e-002	1.69e-005	17.05	0.207	0.521	11.100	0.82	1.11	8.03	57	0
37	c151249.se7	1.10e-001	6.88e-005	9.16	0.331	0.417	9.900	1.10	1.01	11.7	75.2	1
38	c151301.de7	5.92e-002	1.59e-005	15.82	0.227	0.451	11.800	0.84	0.936	12.2	82.3	0
39	c151325.de7	5.99e-002	1.87e-005	15.19	0.245	0.438	11.800	0.85	0.91	13.8	90.1	0
40	c151342.se7	1.30e-001	6.92e-005	8.97	0.281	0.466	9.100	1.10	1.17	7.38	52.4	1
41	c151405.de7	5.23e-002	1.50e-005	17.19	0.243	0.442	12.400	0.82	0.899	14.4	93.4	0
42	c151410.se7	1.15e-001	6.09e-005	9.80	0.299	0.453	9.700	1.10	1.12	8.5	58.1	1
43	c161149.se8	1.37e-001	4.91e-005	11.41	0.192	0.616	8.200	0.94	1.56	3.3	28.5	0
44	c161318.se8	1.16e-001	4.23e-005	12.69	0.210	0.594	8.900	0.94	1.48	4.05	32.7	0
45	c191214.oc8	8.45e-002	1.48e-005	23.18	0.173	0.702	10.500	0.95	1.96	1.87	19.1	0
46	c261219.no7	1.59e-001	2.53e-005	8.15	0.106	0.575	7.200	0.84	1.30	2.98	30.7	0
47	c261330.no7	1.26e-001	2.01e-005	8.96	0.120	0.519	8.100	0.84	1.12	4.45	42	0
48	c271100.oc7	2.50e-001	1.37e-004	5.06	0.178	0.532	6.100	0.95	1.27	4.59	38.8	0
49	c271235.oc7	1.53e-001	7.94e-005	7.66	0.221	0.503	7.800	0.95	1.17	6.67	49.7	1
50	c281153.se8	2.48e-001	1.68e-004	6.07	0.191	0.611	6.000	0.91	1.5	3.65	30.7	1
51	c311908.oc7	5.48e-002	3.32e-005	12.99	0.391	0.342	12.900	0.93	0.712	32.7	181	1
52	c311930.oc7	5.69e-002	2.97e-005	14.76	0.364	0.388	12.800	0.95	0.84	21.4	122	1
53	c311958.oc7	7.22e-002	4.19e-005	12.04	0.355	0.391	11.600	0.99	0.869	18.7	110	1
54	c312021.oc7	5.33e-002	3.00e-005	16.99	0.419	0.398	13.700	1.02	0.906	19.8	108	1
55	c312048.oc7	5.74e-002	3.53e-005	14.76	0.422	0.378	13.200	1.02	0.848	22.7	124	1

^a Records with a value of 1 in the Depth flag column define records classed as at the asymptotic depth limit, as defined in the text.

^b Dates are given in the format, cddtttt.mmy, where dd=day, tttt=time, mm=month, y=year (e.g., c312048.oc7 represents 31 October 1997 at time 20:48).

In recent years wavelet analysis has been applied to surface gravity waves (e.g. Farge, 1992; Foufoula-Georgiou and Kumar, 1994; Mallat, 1998; Torrence and Compo, 1998; Massel, 2001; Huang, 2004). Whereas Fourier analysis sacrifices all temporal information for enhanced frequency resolution, wavelet analysis provides information on the frequency as a function of time, at a cost of some loss of frequency resolution. As such, it is ideal for the analysis of non-stationary processes such as wave breaking or freak waves (e.g. Liu, 1994; Liu and Mori, 2000; Liu and Babanin, 2004). Donelan et al. (1996) extended this approach to an array of wave gauges in the so-called Wavelet Directional Method (WDM).

A complex Morlet wavelet transformation (Grossman and Morlet, 1984) is applied to each of the wave gauges of a spatial array. This

analysis yields a set of wavelet coefficients which are a function of both time and scale (or frequency). If it is assumed that at any instant of time, there is only one wave packet (wavelet) present within the wave array, then the wavenumber vector can be determined by considering the phase difference of the wavelet between the gauges. The phase difference between the gauges i and j is given by (Donelan et al., 1996; Krogstad et al., 2006)

$$\phi_{ij}(t) = k_x(t)X_{ij} + k_y Y_{ij} \quad (11)$$

where (X_{ij}, Y_{ij}) denotes the spatial separation vector between the pair of gauges defined by the array geometry and (k_x, k_y) represents the orthogonal component of the wavenumber vector \underline{k} . Eq. (11) is an

equation in two unknowns, (k_x, k_y) and hence for two or more independent pairs of gauges, this system of equations can be solved. For more than two pairs, the system is over-determined. The resulting solution yields the wavenumber, frequency and direction of each wavelet. Importantly, the solution has not imposed any *a priori* assumptions about a “dispersion” relationship between wavenumber and frequency. The energy spectrum can then be formed by summing the amplitude squared of each of the wavelets within appropriate bins of frequency, wavenumber and direction. As a result it is possible to obtain the directional wavenumber spectrum, $F(k, \theta)$, the directional frequency spectrum, $F(f, \theta)$ and the wavenumber–frequency spectrum (dispersion relationship), $F(k, f)$. In this paper, our interest will be in the omni-directional forms $F(f) = \int F(f, \theta) d\theta$ and $F(k) = \int F(k, \theta) kd\theta$.

The WDM has been extensively reviewed and validated by Krogstad et al. (2006) who compared it with more traditional Fourier approaches to the analysis of directional wave spectra. They concluded that for weakly stationary (a requirement for Fourier analysis) deep water conditions, the WDM produces results consistent with traditional Fourier approaches. In particular, it yields omni-directional frequency spectra almost identical to those obtained from Fourier analysis. Waseda et al. (2008) have also shown that the WDM can recover the directional spectrum of waves generated in a tank to much greater accuracy than alternative methods, such as Maximum Likelihood.

As mentioned in Section 2, the Fourier approach to the representation of the spectrum is problematic in finite depth conditions, where the wave field becomes nonlinear. This nonlinearity manifests itself as a change in shape of the wave profile. Waves in finite depth water typically have peaked crests and flat troughs. The Fourier representation of such a wave form consists of a primary wave at f_p , a harmonic at $2f_p$ and possibly additional harmonics. The harmonic is often described as being phase-locked to the primary wave, as it must propagate at the phase speed of the primary wave to maintain the nonlinear wave profile. Clearly, there are not two waves present, and the harmonic is a mathematical artefact of representing a nonlinear wave profile by the summation of a series of sinusoids. Hence, it is highly likely that the harmonic reported in Part I is such an artefact.

In contrast, the WDM avoids the assumption that the water surface is composed of a summation of sinusoidal components or that there is a particular dispersion relationship relating frequency and wavenumber. The method does, however, assume that only one wavelet is present within the measurement array at any time. Hence, the array

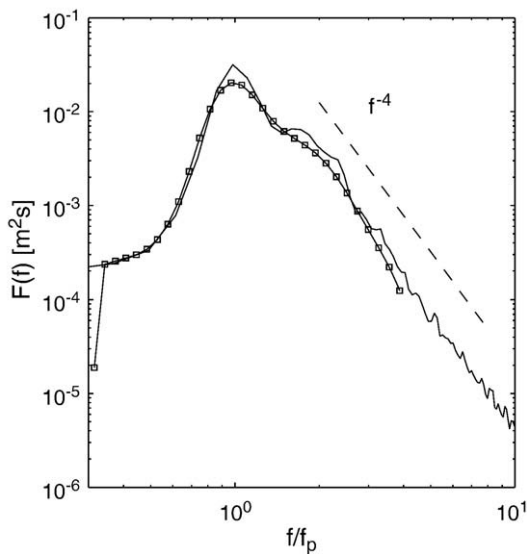


Fig. 2. The omni-directional frequency spectrum, $F(f)$. The WDM form is shown by the squares and the Fourier form by the solid line. Also shown is a f^{-4} reference line.

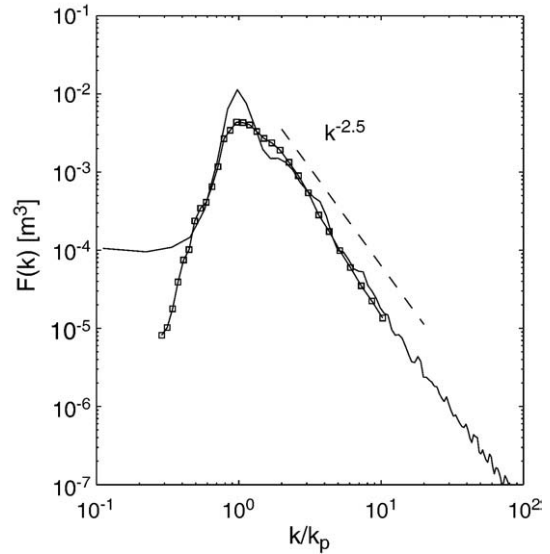


Fig. 3. The omni-directional wavenumber spectrum, $F(k)$. The WDM form is shown by the squares and the Fourier form by the solid line. Also shown is a $k^{-2.5}$ reference line.

should be small compared to the wavelength of the waves being considered.

5. The omni-directional wavenumber spectrum

The WDM was applied to each of the time series in Table 1 and the omni-directional wavenumber, $F(k)$ and frequency, $F(f)$ spectra together with the wavenumber–frequency spectra, $F(k, f)$ were calculated. A typical example of the resulting spectra are shown in Figs. 2–4 (Record c010204.no7 is shown, as in Fig. 4 of Part I). Fig. 2 shows a comparison of the frequency spectrum, $F(f)$ as determined by the WDM and the traditional Fourier analysis of Part I. The WDM cannot resolve the spectrum to as higher frequencies as the Fourier analysis, as it is limited by the spatial separation of the wave gauges. Two significant differences are immediately apparent in this figure. The WDM spectrum has less peak enhancement and the harmonic at $2f_p$ is much less pronounced in the WDM spectrum. Fig. 3 shows a

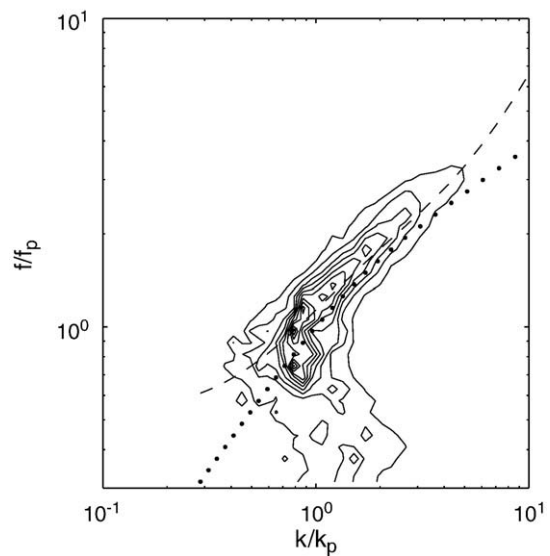


Fig. 4. The wavenumber–frequency spectrum, $F(k, f)$. The spectrum has been normalized, such that the maximum value is 1 and contours have been drawn at 0.9, 0.8, ..., 0.1. The dotted line is the linear dispersion relationship and the dashed line represents the Stokes 3rd order correction Eq. (15) to the dispersion relationship.

comparison of the wavenumber spectrum, $F(k)$ calculated by the WDM and Fourier methods. The Fourier derived wavenumber spectrum was determined from the corresponding frequency spectrum of Fig. 2 since

$$\sigma^2 = \int F(f) df = \int F(k) dk \quad (12)$$

where σ^2 is the variance, and hence

$$F(k) = F(f) \frac{df}{dk}. \quad (13)$$

Assuming the linear dispersion relationship $\omega^2 = gk \tanh(kd)$ yields

$$\frac{df}{dk} = \frac{g}{8\pi^2 f} [\tanh(kd) + kd \operatorname{sech}^2(kd)] \quad (14)$$

It is clear in Fig. 3 that the WDM derived wavenumber spectrum has much less peak enhancement and no apparent harmonic. The WDM spectrum has a much “rounder” shape near the peak than the Fourier form. Both spectra agree well at wavenumbers above approximately 2 to $3k_p$. Assuming the deep water form of the linear dispersion relationship, Eq. (13) suggests that $F(f) \propto f^{-4}$ will yield $F(k) \propto k^{-2.5}$. This result is shown in Fig. 3, the data seeming to decay slightly more rapidly than suggested by the exponent of -2.5 .

Fig. 4 shows the wavenumber–frequency spectrum, $F(k, f)$. The figure shows contours of energy in the two-dimensional wavenumber–frequency domain. The spectrum has been normalized to have a maximum value of 1 and contours have been drawn at [0.9, 0.8, ..., 0.1]. Also shown on the figure is the linear dispersion relationship (dotted line). The data near the peak of the spectrum conform well to the linear dispersion relationship. At higher frequencies (wavenumbers), the data systematically deviates from this relationship. For a given wavenumber, the corresponding frequency is larger than predicted by linear theory. In order to investigate whether this deviation was a result of nonlinear processes, the Stokes 3rd order relationship (Miche, 1944) was calculated

$$\omega^2 = \omega_0^2 \left\{ 1 + \left(\frac{kH}{2} \right)^2 \left[\frac{5 + 2 \cos h(2kd) + 2 \cos h^2(2kd)}{8 \sin h^4(kd)} \right] \right\} \quad (15)$$

where ω_0 is the linear result. This result is strictly applicable to a monochromatic wave and hence is only an approximation to the

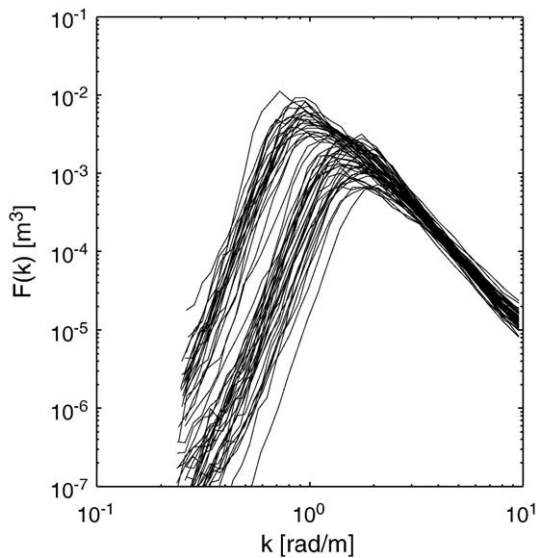


Fig. 5. A composite plot of all wavenumber spectra, $F(k)$ detailed in Table 1. Note the apparently constant level of the high wavenumber region and lack of significant peak enhancement.

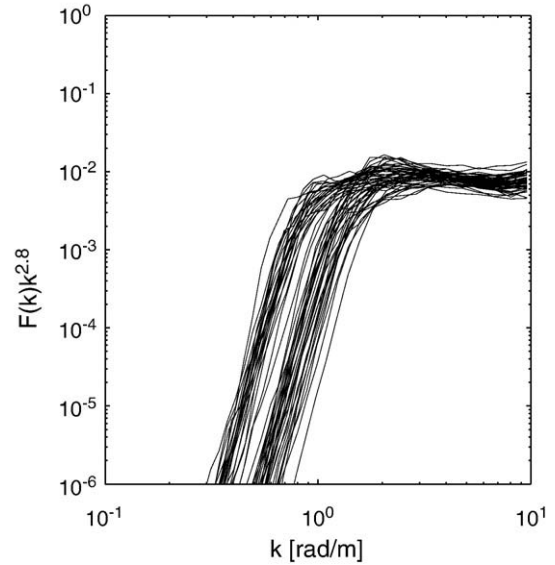


Fig. 6. A composite plot of the wavenumber spectra, as in Fig. 5. The spectra are shown in the form $F(k)k^{2.8}$. Note the apparently constant level of the high wavenumber region and lack of significant peak enhancement.

present case of a full spectrum. Nevertheless, it does represent a reasonable approximation noting the fact that the spectrum is relatively narrow-banded.

Eq. (15) has been plotted in Fig. 4 (dashed line), assuming a water depth, $d = 0.6$ m and a wave height, $H = 0.3$ m, typical of the present data set. As can be seen from the figure, this relationship fits the data remarkably well over the full range of wavenumbers. This result is also consistent with deep-water estimates of the wavenumber–frequency spectra of steep waves obtained by means of the Maximum Likelihood Method (Efimov and Babanin, 1990).

It is also clear that the energy below the spectral peak deviates considerably from the dispersion relationships. At frequencies below the spectral peak, the wavenumber of the components are much larger than one would expect. As a result, the wavenumber spectrum has a much more rapid fall-off below the spectral peak than the corresponding frequency spectrum. This low-frequency energy will appear in the wavenumber spectrum “folded” back into the region immediately above the spectral peak. This possibly accounts for the less peaked form of the wavenumber spectrum. The reason for the significant deviation from the dispersion relation is not clear, but one can speculate that these low frequency waves may have been generated by difference interactions (i.e. $\omega = \omega_2 - \omega_1$) (Longuet-Higgins and Stewart, 1962; Hasselmann et al., 1963; Elgar and Guza, 1985; Herbers et al., 1994; Young and Eldeberky, 1998; Toffoli et al., 2007).

Even though the energy above the spectral peak concentrates along the line of the dispersion shell, there is significant spreading around this shell, both in wavenumber and frequency space. As a result, this will cause a “smearing” of energy across frequency and wavenumber in both $F(f)$ and $F(k)$. Although this occurs across the full spectrum, it is only noticeable near the spectral peak, where the spectrum is most narrow-banded. For a given frequency, the energy will be located over a range of wavenumbers concentrated around the dispersion relationship. This effect appears much more pronounced in the present data than in the deep water results of Efimov and Babanin (1990), Donelan et al. (1996) or Krogstad et al. (2006). It is assumed that the “smearing” observed in the present data is a result of the nonlinearity of the shallow water spectra (note from Table 1, $k_p d$ for the data ranges between 0.8 and 1.3).

Fig. 5 shows a composite plot of all the wavenumber spectra detailed in Table 1. In comparison to typical frequency spectra it is

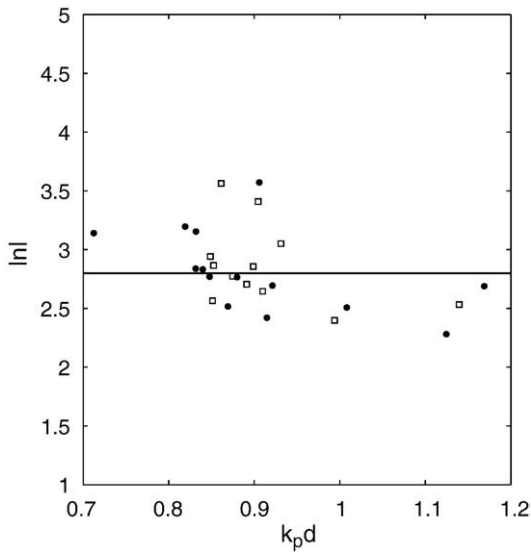


Fig. 7. Values of the exponent n in Eq. (16) as a function of $k_p d$. Data at the asymptotic limit are shown by the solid dots. The horizontal line is drawn at $|n|=2.8$.

obvious that there is little (if any) peak enhancement and that the high wavenumber region of the spectrum appears constant as a function of k_p . This is further examined in Fig. 6, where the form $F(k)k^{2.8}$ is plotted for each of the spectra. The lack of any peak enhancement and the fact that the high wavenumber region of the spectrum can be modelled by a form $\propto Ak^{-2.8}$, where A is a constant, are clear in this figure.

5.1. Parametric spectral form

Based on the results above, a parametric relationship for the wavenumber spectrum of the following form was investigated.

$$F(k) = \beta k_p^{-(3+n)} k^n \exp\left[\frac{n}{4}\left(\frac{k}{k_p}\right)^{-3}\right] \quad (16)$$

Eq. (16) is a modified form of the Pierson–Moskowitz (PM) spectrum (Pierson and Moskowitz, 1964), which was developed to

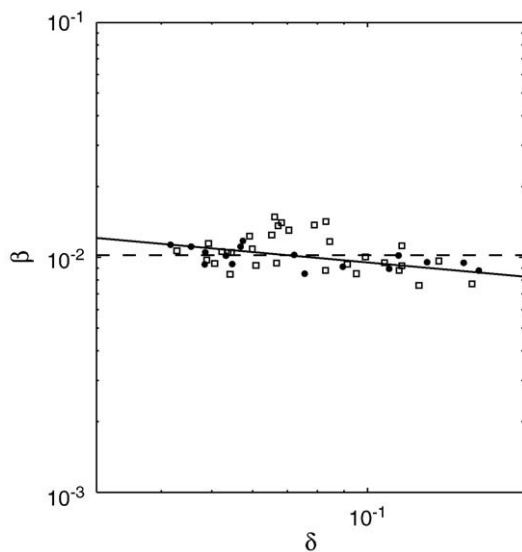


Fig. 8. Values of the parameter β in Eq. (16) as a function of the non-dimensional depth δ . Data at the asymptotic limit are shown by the solid dots. The horizontal dotted line is drawn at the mean value $\beta = 1.02 \times 10^{-2}$. The solid line is the result of the consistency analysis, Eq. (17).

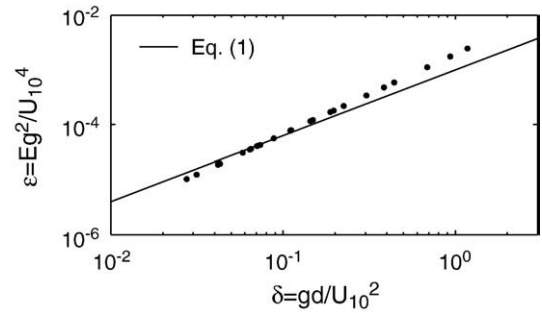


Fig. 9. The non-dimensional energy, ϵ as a function of the non-dimensional water depth, δ . The asymptotic limit defined by Eq. (1) is shown by the solid line. The solid dots show quantities calculated for a range of values of U_{10} and d . Parametric forms of the spectra were calculated for these values and integrated to determine the total energy. A constant value of $\beta = 1.02 \times 10^{-2}$ was assumed for the wavenumber spectrum.

model the deepwater fully developed frequency spectrum. It has been chosen here, because it is a form with no peak enhancement. Alternative forms could have been investigated, particularly for the region below the spectral peak. Relationships of the form of Eq. (16) are, however, commonly used in practice and hence, for simplicity have been adopted here. As well as expressing the relationship in terms of wavenumber, Eq. (16) was also changed compared to the PM form by altering the (k/k_p) exponent to -3 , compared to the original -4 . A value of -4 resulted in a low wavenumber face which consistently decayed more rapidly than the observed data.

Eq. (16) has two free parameters, n , the exponent of decay of the high wavenumber face and β the scale parameter. These parameters were determined using a least-squares fit to the observed spectra. Figs. 7 and 8, show n and β as functions of the nondimensional water depth, $k_p d$ and δ . The spectra considered in this analysis are all in finite depth water, but not all are at the asymptotic depth limit. These asymptotic cases are identified in Table 1 and are shown in Figs. 7 and 8 as the solid dots. The data indicates that the values of both parameters are approximately constant, with $n = -2.8$ and $\beta = 1.02 \times 10^{-2}$. Interestingly, there is no apparent difference between the data at the asymptotic depth limit and the other finite depth cases. Apparently, these parameters are equally applicable for the full data set.

5.2. Consistency analysis

With the constant values of n and β specified above, the wavenumber spectral form, Eq. (16) is fully defined. The asymptotic depth-limited integral parameter relationships Eqs. (1) and (2) are, however, defined over a much larger range of values of nondimensional depth, δ [see Part I] than was available for the spectral fit shown in Figs. 7 and 8. Therefore, it is important to determine whether these values of the spectral parameters yield results consistent with the

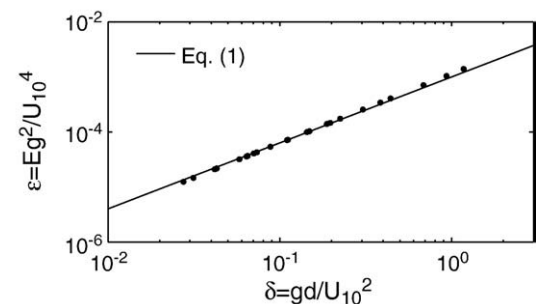


Fig. 10. As for Fig. 9, but β was represented by Eq. (17), $\beta = 6 \times 10^{-3} \delta^{-0.2}$.

integral parameters over this extended parameter range. In order to test this consistency, a range of values of d and U_{10} were defined and the resulting values of δ calculated. For each of these values, κ_p and hence k_p was determined from Eq. (2). With each value of k_p and the stated constant values of n and β , the corresponding spectrum, $F(k)$ was determined. These spectra were integrated to determine the total energy and hence the nondimensional energy, ε . These values were then compared with the predicted values of ε from Eq. (1). This comparison is shown in Fig. 9. As can be seen, there is a consistent deviation from Eq. (1), suggesting that the value of β is not constant over this extended parameter range. The relationship between β and δ was modified to obtain a more consistent result, as shown in Fig. 10. This modified relationship is given by

$$\beta = 6 \times 10^{-3} \delta^{-0.2}. \quad (17)$$

This relationship is plotted in Fig. 8 and gives as consistent a fit to the measured values of β as the previously assumed constant value.

6. Discussion and conclusions

The present analysis has shown significant differences between the wavenumber spectrum determined by the WDM and that inferred from a Fourier analysis. As shown in Fig. 4, this occurs because there is not a “1 to 1” relationship between wavenumber and frequency, as typically assumed by the Fourier analysis. In these finite depth conditions, energy is “smeared” over wavenumbers and frequencies surrounding the dispersion shell. This “smearing” is interpreted as the effects of nonlinearity for these depth-limited conditions. The fact that depth-dependent nonlinear processes are active is obvious from the Fourier frequency spectrum, where a clear harmonic can be seen. The WDM analysis confirms that this harmonic represents energy bound to the spectral peak and not conforming to the dispersion relationship. As a result of the nonlinear processes, the WDM derived wavenumber form has a much less peaked (rounder) spectral form than the inferred Fourier form. Also, there is no harmonic apparent in the WDM wavenumber form, again confirming that this “peak” represents energy bound to the spectral peak. Krogstad et al. (2006) have compared WDM and Fourier spectra in deep water and found good agreement at the spectral peak. This result adds strength to the suggestion that the differences observed in the present data set are the result of depth-induced nonlinearity.

In addition to the depth-induced nonlinearities at low wavenumbers, the high wavenumber region of the spectrum, where the local components become steep, also shows nonlinearity. As a result, these components deviate from the linear dispersion relationship. The data do, however, agree remarkably well with the 3rd order result of Miche (1944). This deviation from the linear result at high wavenumbers has also been observed in deep water by Efimov and Babanin (1990) and Krogstad et al. (2006).

As shown in Figs. 6 and 7, the wavenumber spectrum has a high wavenumber form proportional to $k^{-2.8}$, although there is clear scatter in the value of the exponent as has been clear in previous measurements of the frequency spectrum (e.g. Liu, 1989; Young et al., 1996). The value of the exponent (i.e. -2.8) is larger in magnitude than one might initially expect. Miller and Vincent (1990) have proposed a form proportional to $k^{-2.5}$, based on transforming a frequency spectrum of the form f^{-4} (as observed for this data set by Young and Babanin, 2006). As already noted above, the data do deviate from the linear dispersion relationship and hence a deviation from a value of -2.5 is not surprising. Indeed, as the high frequency (wavenumber) exponent is the result of the balance between the various physical processes (atmospheric input, nonlinear interaction, wave breaking and bottom friction), a variety of values may well be possible, depending on the relative balance at a particular time. This may account for some of the scatter apparent in Fig. 7.

The present analysis has clearly shown that the wavenumber spectrum is superior to the frequency spectrum in representing finite depth wind generated waves. The form represented by Eqs. (16) and (17) fully defines the asymptotic depth-limited wind wave spectrum in a far simpler manner than was possible for the frequency spectrum [e.g. Part I]. There is also evidence that this form may be applicable to finite depth spectra which are not at the asymptotic limit [e.g. Figs. 7 and 8 show no difference for data at the asymptotic limit and other finite depth data]. The present data set cannot, however, define the parameter range over which the form may be applicable. Clearly, it is not a universal form, as the deep water limit is quite different to Eq. (16) near the spectral peak.

Finally, the analysis has clearly shown the power of the WDM in analysing finite depth data. The nonlinear nature of the data means that the assumption of any dispersion relationship is problematic. In such circumstances, the WDM represents a powerful method for the direct determination of the wavenumber spectral form.

Acknowledgements

The authors gratefully acknowledge the financial support of the U.S. Office of Naval Research (grants N00014-97-1-0234, N00014-97-1-0277 and N0014-97-1-0233) and the Australian Research Council (grant A00102965). We also express our gratitude to the staff and students of the School of Civil Engineering of the Australian Defence Force Academy: Jim Baxter, Karl Shaw, Ian Shephard and Michael Wilson who offered highly professional and prompt responses to all urgent demands during the experiments.

References

- Alpers, W.R., Ross, D.B., Rufenach, C.L., 1981. On the detectability of ocean surface waves by real and synthetic aperture radar. *J. Geophys. Res.* 86, 6481–6498.
- Banner, M.L., Jones, I.S.F., Trinder, J.C., 1989. Wavenumber spectra of short gravity waves. *J. Geophys. Res.* 73, 513–530.
- Bottema, M., 2007. Measured wind-wave climatology Lake IJssel (NL). Report RWS RIZA 2007.020. ISBN: 978-90-369-1399-7. 278 pp.
- Bouws, E., Günther, H., Rosenthal, W., Vincent, C.L., 1985. Similarity of the wind wave spectrum in finite depth water, 1. Spectral form. *J. Geophys. Res.* 90, 975–986.
- Bouws, E., Günther, H., Rosenthal, W., Vincent, C.L., 1987. Similarity of the wind wave spectrum in finite depth water, 2. Statistical relationships between shape and growth stage parameters. *Dtsch. Hydrogr. Z.* 40, 1–24.
- Bretschneider, C.L., 1958. Revisions in wave forecasting: deep and shallow water. Proc. 2nd Conf. on Coastal Eng. ASCE, Council on Wave Research.
- Donelan, M.A., Drennan, W.M., Magnusson, A.K., 1996. Nonstationary analysis of the directional properties of propagating waves. *J. Phys. Oceanogr.* 26, 1901–1914.
- Efimov, V.V., Babanin, A.V., 1990. Nonlinear effects in the wind wave spectrum. *Izv. Atmos. Ocean. Phys.* 26 (2), 133–138.
- Elgar, S., Guza, R.T., 1985. Observations of bispectra of shoaling surface gravity waves. *J. Fluid Mech.* 161, 425–448.
- Farge, M., 1992. Wavelet transforms and their applications to turbulence. *Annu. Rev. Fluid Mech.* 24, 395–457.
- Foufoula-Georgiou, E., Kumar, P. (Eds.), 1994. Wavelets in Geophysics. Academic Press, San Diego, CA. 372 pp.
- Grossman, A., Morlet, J., 1984. Decomposition of Hardy functions into square integrable wavelets of constant slope. *SIAM J. Math. Anal.* 15 (4), 723–736.
- Hasselmann, K., Munk, W., MacDonald, G., 1963. Bispectra of ocean waves. In: Rosenblatt, M. (Ed.), *Time Series Analysis*. John Wiley, New York, pp. 125–139.
- Hasselmann, K., Raney, R.K., Plant, W.J., Alpers, W., Schuchman, R.A., Lyzenga, D.R., Rufenach, C.L., Tucker, M.J., 1985. Theory of synthetic aperture radar ocean imaging — a MARSEN view. *J. Geophys. Res.* 90, 4659–4686.
- Herbers, T.H., Elgar, S., Guza, R.T., 1994. Infragravity-frequency (0.005–0.05 Hz) motions on the shelf. Part I: Forced waves. *J. Phys. Oceanogr.* 24, 917–927.
- Holthuijsen, L.H., 1983. Observations of the directional distribution of ocean-wave energy in fetch-limited conditions. *J. Phys. Oceanogr.* 13, 191–207.
- Huang, M.C., 2004. Wave parameters and functions in wavelet analysis. *Ocean Eng.* 31 (1), 111–125.
- Kitaigorodskii, S.A., 1983. On the theory of the equilibrium range in the spectrum of wind-generated gravity waves. *J. Phys. Oceanogr.* 13, 816–827.
- Kitaigorodskii, S.A., Krasitskii, V.P., Zaslavskii, M.M., 1975. On Phillips' theory of equilibrium range in the spectra of wind-generated gravity waves. *J. Phys. Oceanogr.* 5, 410–420.
- Krogstad, H.E., Magnusson, A.K., Donelan, M.A., 2006. Wavelet and local analysis of ocean waves. *Int. J. Offshore Polar Eng.* 16 (2), 97–103.
- Liu, P.C., 1989. On the slope of the equilibrium range in the frequency spectrum of wind waves. *J. Geophys. Res.* 94, 5017–5023.
- Liu, P.C., 1994. Wavelet spectrum analysis and ocean wind waves. In: Foufoula-Georgiou, E., Kumar, P. (Eds.), *Wavelets in Geophysics*. Academic Press, CA, pp. 151–166.

- Liu, P.C., Babanin, A.V., 2004. Using wavelet spectrum analysis to resolve breaking events in the wind wave time series. *Ann. Geophys.* 22, 3335–3345.
- Liu, P.C., Mori, N., 2000. Characterizing freak waves with wavelet transform analysis. In: Olagnon, M., Athanassoulis, G.A. (Eds.), *Rogue Waves 2000*. IFREMER, Plouzane, pp. 151–155.
- Longuet-Higgins, M.S., Stewart, R.W., 1962. Radiation stress and mass transport in gravity waves with application to “surf beats”. *J. Fluid Mech.* 17, 459–480.
- Mallat, S., 1998. *A wavelet tour of signal processing*. Academic Press, San Diego, CA, 577 pp.
- Massel, S.R., 2001. Wavelet analysis for processing of ocean surface wave records. *Ocean Eng.* 28, 957–987.
- Miche, M., 1944. Mouvements ondulatoires de la mer en profondeur constante ou décroissante. *Ann. Ponts Chaussees* 114, 25–78.
- Miller, H.C., Vincent, C.L., 1990. FRF spectrum: TMA with Kitaigorodskii's f^{-4} scaling. *ASCE J. Waterw. Port Coast. Ocean Div.* 116, 57–78.
- Phillips, O.M., 1985. Spectral and statistical properties of the equilibrium range in wind-generated gravity waves. *J. Fluid Mech.* 156, 505–531.
- Pierson, W.J., Moskowitz, L., 1964. A proposed spectral form for fully developed wind seas based on the similarity theory of S.A. Kitaigorodskii. *J. Geophys. Res.* 69, 5181–5190.
- Resio, D.T., 1988. Shallow-water waves. II: Data comparisons. *J. Waterw. Port Coast. Ocean Eng.* 114 (1), 50–65.
- Resio, D.T., Pihl, J.H., Tracy, B.A., Vincent, C.L., 2001. Nonlinear energy fluxes and the finite depth equilibrium range in wave spectra. *J. Geophys. Res.* 106, 6985–7000.
- Resio, D.T., Long, C.E., Vincent, C.L., 2004. Equilibrium-range constant in wind-generated wave spectra. *J. Geophys. Res.* 109 (C01018). doi:10.1029/2003JC001788.
- Smith, J.M., Vincent, C.L., 1992. Shoaling and decay of two wave trains on a beach. *J. Waterw. Port Coast. Ocean Eng.* 118, 517–533.
- Smith, J.M., Vincent, C.L., 2002. Application of spectral equilibrium ranges in the surf zone. *Proc. 28th Int. Conf. on Coast Eng.* World Scientific, pp. 269–279.
- Thijssse, J.Th., 1949. Dimensions of wind-generated waves. *General Assembly of Association d'Océanographie Physique. Procès-Verbaux*, vol. 4, pp. 80–81. Oslo.
- Thompson, E.F., 1980. Energy spectra in shallow U.S. coastal waters. *Coastal Engineering Research Center, Tech. Paper 80-2*, Ft. Belvoir, Va. 149 pp.
- Toffoli, A., Onorato, M., Babanin, A.V., Bitner-Gregersen, E., Osborne, A.R., Monbaliu, J., 2007. Second-order theory and setup in surface gravity waves: a comparison with experimental data. *J. Phys. Oceanogr.* 37, 2726–2739.
- Torrence, C., Compo, G.P., 1998. A practical guide to wavelet analysis. *Bull. Am. Meteorol. Soc.* 79 (1), 61–78.
- U.S. Army Corps of Engineers, 1955. *Waves and wind tides in shallow lakes and reservoirs*. Summary Report, Project CW-167, Jacksonville District, Fla.
- Vincent, C.L., 1984. Shallow water waves — a spectral approach. *Int. Conf. on Coastal Eng.* ASCE, Houston, Texas, pp. 370–382.
- Vincent, C.L., 1985. Depth-controlled wave height. *J. Waterw. Port Coast. Ocean Eng.* 111 (3), 459–475.
- Waseda, T., Kinoshita, T., Tamura, H., 2008. Evolution of a random directional wave and freak wave occurrence. *J. Phys. Oceanogr.* 38. doi:10.1175/2008JPO4031.1.
- Young, I.R., 1999. *Wind Generated Ocean Waves*. Elsevier Sciences Ltd. 0-08-043317-0, 306 pp.
- Young, I.R., Babanin, A.V., 2006. The form of the asymptotic depth-limited wind-wave frequency spectrum. *J. Geophys. Res.* 111 (C06031). doi:10.1029/2005JC003398.
- Young, I.R., Eldeberky, Y., 1998. Observations of triad coupling of finite depth wind-waves. *Coast. Eng.* 33, 137–154.
- Young, I.R., Verhagen, L.A., 1996a. The growth of fetch limited waves in water of finite depth. Part I: Total energy and peak frequency. *Coast. Eng.* 28, 47–78.
- Young, I.R., Verhagen, L.A., 1996b. The growth of fetch limited waves in water of finite depth. Part II: Spectral evolution. *Coast. Eng.* 28, 79–100.
- Young, I.R., Rosenthal, W., Ziemer, F., 1985. A three-dimensional analysis of marine radar images for the determination of ocean wave directionality and surface currents. *J. Geophys. Res.* 90 (C1), 1049–1060.
- Young, I.R., Verhagen, L.A., Khatri, S.K., 1996. The growth of fetch limited waves in water of finite depth. Part III: Directional spectra. *Coast. Eng.* 28, 101–122.
- Young, I.R., Banner, M.L., Donelan, M.A., Babanin, A.V., Melville, W.K., Veron, F., McCormick, C., 2005. An integrated system for the study of wind-wave source terms in finite-depth water. *J. Atmos. Ocean. Technol.* 22 (7), 814–831.
- Zakharov, V., 1999. Statistical theory of gravity and capillary waves on the surface of a finite-depth fluid. *Eur. J. Mech. B/Fluids* 18, 327–344.